

# Large-scale molecular dynamics simulations of alkanethiol self-assembled monolayers

Satyavani Vemparala and Bijaya B. Karki

*Biological Computation and Visualization Center, Department of Physics & Astronomy and Department of Computer Science, Louisiana State University, Baton Rouge, Louisiana 70803*

Rajiv K. Kalia, Aiichiro Nakano, and Priya Vashishta

*Collaboratory for Advanced Computing and Simulations, Department of Materials Science & Engineering, Department of Computer Science, Department of Physics & Astronomy and Department of Biomedical Engineering, University of Southern California, Los Angeles, California 90089-0242*

(Received 20 May 2003; accepted 2 June 2004)

Large-scale molecular dynamics simulations of self-assembled alkanethiol monolayer systems have been carried out using an all-atom model involving a million atoms to investigate their structural properties as a function of temperature, lattice spacing, and molecular chain length. Our simulations show that the alkanethiol chains of 13-carbons tilt from the surface normal by a collective angle of  $25^\circ$  along next-nearest-neighbor direction at 300 K. The tilt structure of 13-carbon alkanethiol system is found to depend strongly on temperature and exhibits hysteresis. At 350 K the 13-carbon alkanethiol system transforms to a disordered phase characterized by small collective tilt angle, flexible tilt direction, and random distribution of backbone planes. The tilt structure also depends on lattice spacing: With increasing lattice spacing  $a$  the tilt angle increases rapidly from a nearly zero value at  $a=4.7 \text{ \AA}$  to as high as  $34^\circ$  at  $a=5.3 \text{ \AA}$  at 300 K for 13-carbon alkanethiol system. Finally, the effects of the molecular chain length on the tilt structure are significant at high temperatures.

© 2004 American Institute of Physics. [DOI: 10.1063/1.1775779]

## I. INTRODUCTION

Self-assembled monolayers (SAMs) of functionalized long-chain molecules on the surface of solid substrates have been the subject of extensive theoretical and experimental research<sup>1</sup> due to their broad range of applications in mechanical (e.g., lubrication<sup>2</sup>), chemical, electronic, and biotechnological fields. Self-assembly of organic films are attractive in diverse fields due to the possibility of tuning their properties by selectively modifying specific functional groups (i.e., end groups) without modifying the entire chain. For instance, by changing just the end group of alkanethiol-based monolayer [e.g.,  $S(\text{CH}_2)_n\text{CH}_3$ ] from  $\text{CH}_3$  to  $\text{OH}$ , the property of the resulting chemical surface can be varied from hydrophobic to hydrophilic. Oligo-ethylene-glycol-terminated alkanethiol SAMs exhibit interesting protein adsorption properties<sup>3</sup> and as such are useful for interfacing biological materials with inorganic surfaces. For example, it is possible to immobilize a single biomolecule or an array of biomolecules on the surface of SAMs for biosensor applications.

SAMs can be formed by spontaneous adsorption of different types of molecules from solution onto a variety of solid substrates, such as gold, silver, and hydroxylated silicon. Alkanethiols on Au(111) surface are most widely studied mainly because gold does not have a stable oxide and hence can be handled in ambient conditions. Infrared spectroscopy studies have established that the alkanethiol chains tilt on average by  $30 \pm 10^\circ$ .<sup>4,5</sup> Earlier experimental studies showed that this system forms a well-ordered  $(\sqrt{3} \times \sqrt{3})R30^\circ$  triangular lattice with lattice constant  $a=4.97$

$\pm 0.05 \text{ \AA}$  with one chain per unit cell,<sup>6,7</sup> and subsequent experiments observed superlattice structures, superimposed on the triangular lattice, such as two-chain<sup>8</sup> and four-chain unit cell  $C(4 \times 2)$  reconstructions.<sup>9-12</sup> Ulman *et al.*<sup>13</sup> used grazing angle Fourier transform infrared spectroscopy to compare monolayers on gold and silver surfaces, and the spectra from silver surface ( $a=4.65 \pm 0.15 \text{ \AA}$ ) suggests that the tilt angle is much smaller ( $\sim 6^\circ-7^\circ$ ) than that on gold. This suggests a strong dependence of tilt structure of SAMs on substrate.

SAMs exhibit rather complex structural and dynamical behaviors, which are not well understood. Although the molecular chains show collective tilt away from the surface normal, the atomistic details of tilt structure are not known. Computer simulations can provide a theoretical basis for answering some of the questions as well as interpreting experimental results. Molecular dynamics (MD) and Monte Carlo methods were previously used to simulate SAMs of alkanethiol molecules chemisorbed on gold substrate.<sup>14-18</sup> Although these studies have given significant insight into various properties of SAMs, the simulated system sizes are relatively small ( $<5000$  atoms or 100 chains) and many of these simulations are based on united-atom models, where  $\text{CH}_2$  and  $\text{CH}_3$  units are treated as single sites. In this paper, we report a large-scale MD study of alkanethiol SAM with system size up to a million atoms based on an all-atom model (hydrogen atoms are treated explicitly). We study structural properties of the SAMs as a function of temperature, lattice spacing, and molecular chain length. Most of the results obtained in this paper are for 13-carbon length chain system.

The paper is organized as follows. In Sec. II we describe the force field used for simulations of alkanethiols along with a brief description of the MD algorithm used and the initial setup of the system. Section III describes the results of the simulations including the effect of temperature, lattice constant, and molecular chain length. Section IV contains the conclusions of this study.

## II. METHODOLOGY

In MD simulations the physical system is represented by a set of  $N$  atoms. We follow the trajectory, i.e., positions,  $\{\vec{r}_i = 1, \dots, N\}$ , and velocities,  $\{\vec{v}_i = 1, \dots, N\}$ , of all the atoms by numerically integrating the Newton's equations of motion,

$$m_i \frac{d^2 \vec{r}_i}{dt^2} = \vec{F}_i, \quad (1)$$

where  $m_i$  is the mass of atom  $i$  and the force on atom  $i$  is defined as

$$\vec{F}_i = - \frac{\partial V(\{\vec{r}_i\})}{\partial \vec{r}_i}. \quad (2)$$

The interatomic potential energy  $V$  encodes interactions among atoms and therefore is the essential ingredient of MD simulations.

### A. Interatomic potential model

We use the interatomic potential model in which the conformational energy ( $V$ ) of a molecular system is split into bonded, nonbonded, and surface interaction energies:

$$V = V_{\text{bonded}} + V_{\text{nonbonded}} + V_{\text{surface}}. \quad (3)$$

Here  $V_{\text{bonded}}$  represents the bonded interactions that arise from bond-stretching, bending, and torsions:

$$V_{\text{bonded}} = \sum_{ij} \frac{1}{2} k_{ij}^s (r_{ij} - r_{ij}^0)^2 + \sum_{ijk} \frac{1}{2} k_{ijk}^b (\alpha_{ijk} - \alpha_{ijk}^0)^2 + \sum_{ijkl} \frac{1}{2} k_{ijkl}^t [1 + \cos 3(\phi_{ijkl} - \phi_{ijkl}^0)], \quad (4)$$

where two atoms  $i$  and  $j$  define a covalent bond of length  $r_{ij}$ ; three atoms  $i, j$ , and  $k$  define bond angle  $\alpha_{ijk}$ , and four atoms  $i, j, k$ , and  $l$  define a dihedral angle  $\phi_{ijkl}$ . A pair of atoms  $i$  and  $j$  are considered to be nonbonded if they belong to different molecules or are separated by more than three bonds in the same molecule. The resulting nonbonded interactions (i.e., long-range repulsions and van der Waals interactions) are expressed as

$$V_{\text{nonbonded}} = \sum_{i < j} [A_{ij} \exp(-B_{ij} r_{ij}) - C_{ij} r_{ij}^{-6}], \quad (5)$$

which are truncated at a cutoff radius of  $r_c = 9.0 \text{ \AA}$ :

$$V_{\text{nonbonded}}(r) = V_{\text{nonbonded}}(r) - V_{\text{nonbonded}}(r_c) - (r - r_c) \left. \frac{dV_{\text{nonbonded}}}{dr} \right|_{r=r_c}. \quad (6)$$

Finally, the interactions of sulfur and carbon atoms with gold substrate (i.e., surface interactions) are modeled<sup>14</sup> by

TABLE I. Force field parameters.

$ij$	$r_{ij}^0$ (Å)	$k_{ij}^s$ (kcal/mol/Å <sup>2</sup> )		
C-C	1.53	617.8		
H-H	1.09	655.2		
$ijk$	$\alpha_{ijk}^0$ (rad)	$k_{ijk}^b$ (kcal/mol/rad <sup>2</sup> )		
C-C-C	1.9373	107.6		
C-C-H	1.9106	85.8		
H-C-H	1.8832	77.0		
$ijkl$	$\phi_{ijkl}^0$ (rad)	$k_{ijkl}^t$ (kcal/mol/rad <sup>2</sup> )		
C-C-C-H	0	0.277 92		
H-C-C-H	0	0.277 92		
C-C-C-C	0	0.277 92		
$ij$	$A_{ij}$ (kcal/mol)	$B_{ij}$ (1/Å)	$C_{ij}$ (Å <sup>6</sup> kcal/mol)	
C-C	14 976.0	3.09	640.8	
H-H	2649.6	3.74	27.4	
C-H	4320.0	3.42	138.2	
S-S	79 937.0	3.18	2002.0	
S-C	34 599.7	3.13	1132.6	
S-H	14 553.4	3.45	234.2	
	$k_2^{\text{SF}}$ (kcal/mol)	$k_{12}^{\text{SF}}$ (kcal/mol/Å <sup>12</sup> )	$k_3^{\text{SF}}$ (kcal/mol/Å <sup>3</sup> )	$z^0$ (Å)
S	10.0	81 289	359	0.269
C	0.0	55 664	27.4	0.860

$$V_{\text{surface}} = \sum_s \frac{1}{2} k_s^{\text{SF}} d_s^2 + \sum_{pq} \left[ \frac{k_{12}^{\text{SF}}}{(z_{pq} - z_p^0)^{12}} - \frac{k_3^{\text{SF}}}{(z_{pq} - z_p^0)^3} \right], \quad (7)$$

where the index  $s$  runs over sulfur atoms,  $p$  counts the number of chains or molecules,  $q$  runs over sulfur and carbon atoms on each molecule, and  $d_s$  is the distance of sulfur atom from its original position on  $x$ - $y$  plane. The first term constrains the motion of sulfur atoms on  $x$ - $y$  surface whereas the second term involves  $z$  positions of sulfur and carbon atoms. The model parameters<sup>14,19,20</sup> used in our MD simulations are given in Table I.

### B. Multiple-time-scale molecular dynamics

In previous MD simulations,<sup>14–16</sup> the nearest-neighbor distances were fixed, based on an iterative procedure. Because of the sequential nature of the iterative procedure, parallelization of this approach is nontrivial and accordingly poses difficulty in simulating large systems. To simulate large organic macromolecular systems such as SAMs, we have developed a parallel MD algorithm that uses a divide-and-conquer strategy based on spatial decomposition and dynamic management of linked-cell lists and bonded-atom lists.<sup>21,22</sup> Our algorithm uses a penalty function based approach [see the first term in Eq. (4)] coupled with multiple time-scale (MTS) method to impose bond-length constraints. The bonded interactions vary much more rapidly than the nonbonded interactions and the time step of integration,  $\Delta t$ , needs to be chosen smaller than the smallest time scale. The MTS method reduces the number of force computations significantly by separating the fast (small time-scale) modes from the slow (large time-scale) modes. We use an MTS

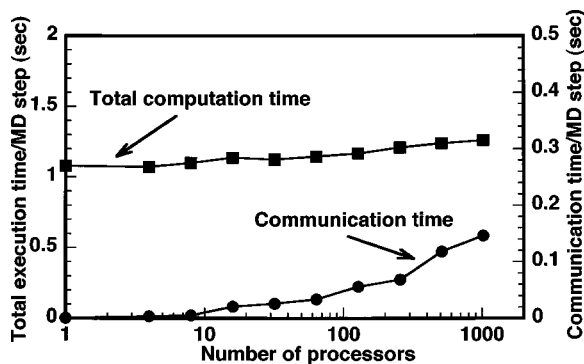


FIG. 1. The scalability test result on a system of SAMs of size of  $21.6 \times 10^6$  atoms on 1024 SP4 processors.

algorithm called rRESPA,<sup>23,24</sup> which is reversible since it is based on the symmetric Trotter expansion of the time evolution operator. The rRESPA algorithm is also symplectic, i.e., the phase space volume is a loop invariant, which results in long time stability of solutions. We use two different time steps of 0.3 and 3.0 fs for the bonded (including surface) and nonbonded interactions, respectively. By computing nonbonded interactions less frequently than bonded interactions, the performance of the code has been sped up by a factor of 4. The Newton's equations of motion are integrated using the velocity Verlet algorithm<sup>21</sup> within the rRESPA scheme:

$$\vec{r}_i(t + \Delta t) = \vec{r}_i(t) + \vec{v}_i(t)\Delta t + \frac{1}{2} \left( \frac{\vec{F}_i(t)}{m_i} \right) \Delta t^2 + O(\Delta t^3) \quad (i = 1, \dots, N), \quad (8)$$

$$\vec{v}_i(t + \Delta t) = \vec{v}_i(t) + \frac{1}{2} \left( \frac{\vec{F}_i(t + \Delta t) + \vec{F}_i(t)}{m_i} \right) \Delta t + O(\Delta t^3) \quad (i = 1, \dots, N). \quad (9)$$

We have recently performed scalability tests of our parallel MD algorithm<sup>25</sup> on an IBM SP4 computer and achieved 90% of the perfect speedup on 1024 processors (see Fig. 1).

### C. Initial setup

The system of self-assembled monolayers consists of a triangular lattice of sulfur atoms, bonded to a substrate, which are the head group atoms of  $S(\text{CH}_2)_n\text{CH}_3$  chains, where  $n$  is varied from 7 to 25. (Most of the results in the following sections are for  $n = 13$ .) The lattice spacing  $a$  of the triangular lattice is also varied from 4.7 to 5.3 Å. To study the size effect in our MD simulations, we consider two lateral system sizes, one comprising of  $26 \times 44 = 2288$  chains and the other comprising of  $80 \times 144 = 23\,040$  chains. The  $x$  and  $y$  dimensions of the MD box corresponding to these systems are  $225.17 \times 220$  and  $692.82 \times 720$  Å, respectively (see Fig. 2). Periodic boundary conditions are applied in the surface plane. In order to remove interactions between periodic images in  $z$  direction, a vacuum space (longer than  $r_c$ ) is inserted above the free surface of the SAM.

A tilted alkanethiol chain is characterized by tilt angle ( $\theta$ ), twist angle ( $\phi$ ), and tilt direction ( $\chi$ ), see Fig. 3. An initial angle of  $\theta \sim 2^\circ$  is given to all the molecular chains, and

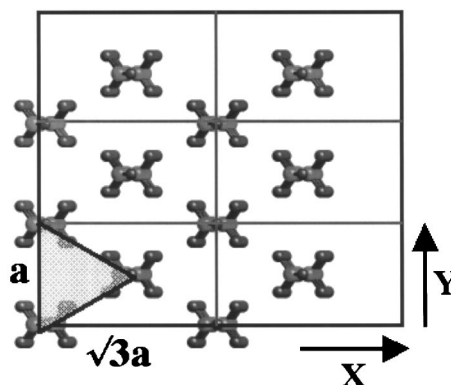


FIG. 2. Schematic of the triangular lattice (lattice constant= $a$ ) of the alkanethiol system in  $xy$  plane.

the backbone planes of all the chains are rotated by  $\phi \sim 2^\circ$  with next-nearest-neighbor direction (parallel to  $x$  axis) to break the symmetry of the triangular lattice, which gives an initial tilt direction of  $\sim 2^\circ$ . The conformation of each chain is chosen such that, the backbone plane of each chain is in an *all-trans* structure.

All the atoms are given random initial velocities, according to the Maxwell-Boltzmann distribution, corresponding to temperature of  $T = 300$  K. We thermalize the system for 150 ps during which the molecular chains increasingly tilt away from the surface normal towards one of the next-nearest-neighbor directions and the tilt structure finally reaches a steady state (Fig. 4). The statistical averages of potential energies and structural parameters are calculated, after the thermalization stages, over the next 50 ps.

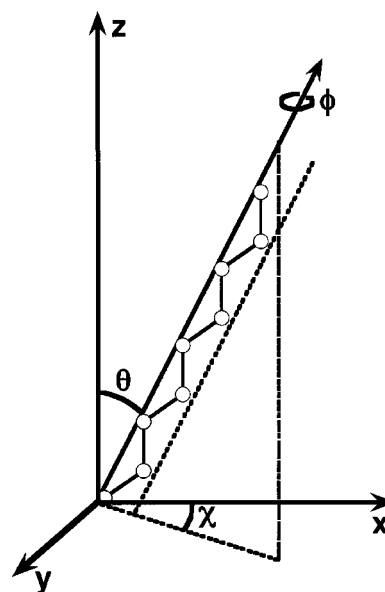


FIG. 3. Schematic representation of a tilted alkanethiol molecule:  $\theta$  is the tilt angle of the molecule away from the surface normal,  $\chi$  is the precession angle about the surface normal that represents the tilt direction, and  $\phi$  is the twist (rotation about the molecular axis) angle that defines the orientation of the chain backbone plane relative to the tilt direction.

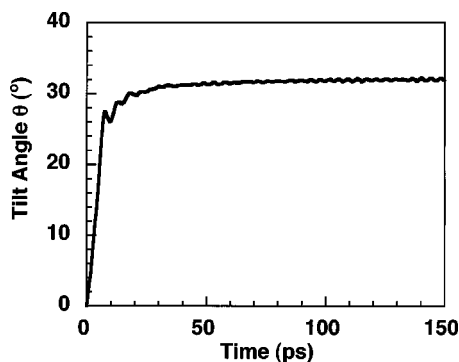


FIG. 4. Time evolution of the collective tilt structure during thermalization for  $n=13$ .

### III. RESULTS AND DISCUSSION

#### A. Effect of temperature

We have studied the effect of temperature on the structure of the alkanethiol system with chain length  $n=13$ , lattice constant  $a=5 \text{ \AA}$ , and the number of atoms is 100 672 (2288 chains). Starting from the initially thermalized system (in which the temperature saturated to a value of 150 K), we successively scale the atom velocities to vary the system temperature from 150 to 500 K in steps of 50 K. For each 50 K step, the temperature is increased over 30 ps, the system is thermalized for 50 ps, and statistical averages obtained over another 50 ps. To study possible hysteresis, the temperature is decreased from 500 to 200 K. We also obtain the 0 K system by gradually decreasing the temperature from the initially thermalized system.

As shown in Fig. 5(a), with increasing temperature, the average tilt angle ( $\theta$ ) of the chains initially decreases slowly and then rapidly until it saturates at a low value for temperatures higher than 350 K. At 300 K the calculated tilt angle ( $25^\circ$ ) agrees fairly well with experimental tilt angle of  $30 \pm 10^\circ$  (Refs. 8 and 12) and  $33.7 \pm 0.8^\circ$  (Refs. 9 and 12), which was measured for  $n=12$  using grazing incidence x-ray diffraction. The tilt direction is along the next-nearest-neighbor (NNN) direction ( $\chi \sim 0$ ) below 300 K and at temperatures above 300 K, it shifts away from the NNN direction by about  $15^\circ$  [see Fig. 5(b)]. However, the system does not show any clear precession about the surface normal even at very high temperatures. This is in contrast to previous MD studies based on united atom model,<sup>14,16</sup> in which the tilt direction was no longer locked at  $T > 300 \text{ K}$ . The tilt angle and tilt direction obtained in our studies is similar to the values obtained in Ref. 18 where united atom model was employed. Figure 5(a) also shows the results of million atom MD simulations, which are nearly identical to hundred thousand atom system, showing negligible effect of system size. Figure 5(a) also shows the presence of a hysteresis between 250 and 350 K. The temperature range over which the order is lost is small compared to the previous simulations<sup>14</sup> and experiments.<sup>26</sup> The possible reasons are the use of explicit hydrogen model, surface potential model used in the simulations.

The twist angle ( $\phi$ ) distribution is found to change dramatically with temperature (Fig. 6). At low temperatures, the

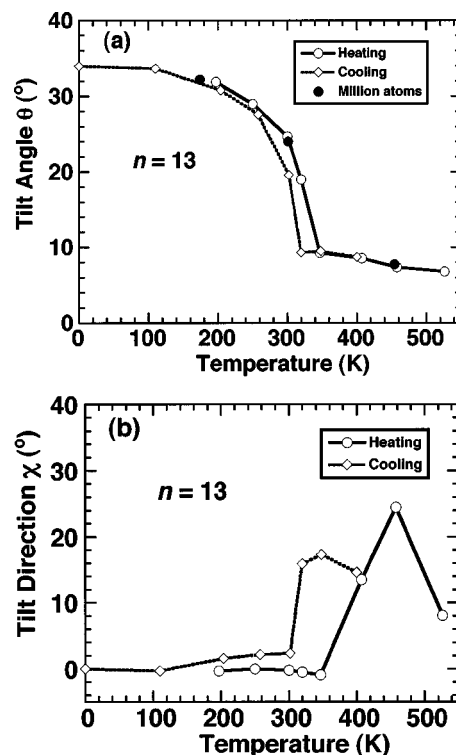


FIG. 5. (a) Temperature variation of the collective tilt angle: The simulation results from heating run and cooling run are shown by circles and diamonds, respectively, for the systems of a hundred thousand (open symbols) and a million atoms (solid symbols) for  $n=13$ . (b) Temperature variation of tilt direction: The simulation results from heating run and cooling run are shown by circles and diamonds, respectively.

twist angle distribution has two major peaks (i.e., the molecular backbone planes have two well-defined orientations with twist angles at  $\pm 50^\circ$  with respect to tilt direction) and two minor peaks at  $\pm 130^\circ$ . This is consistent with the experimental result of  $46^\circ$  at 160 K and for  $n=18$ .<sup>27</sup> With increasing temperature, the minor peaks grow to some extent but the major peaks diminish substantially. The resulting uniform four-site distribution pattern at 300 K is similar to that observed in crystalline  $n$ -alkane systems.<sup>28</sup> These peaks disappear above 400 K, and the resulting flat distribution indicates that the system evolves from a phase in which individual chains are locked in their orientation to a phase where chains are free to rotate about their molecular axes.

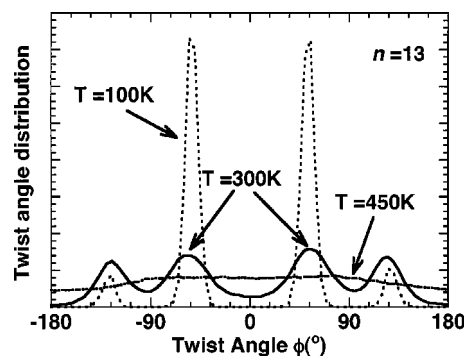


FIG. 6. Calculated twist angle distribution plotted as a function of twist angle at  $T=100, 300,$  and  $450 \text{ K}$  for  $n=13$ .

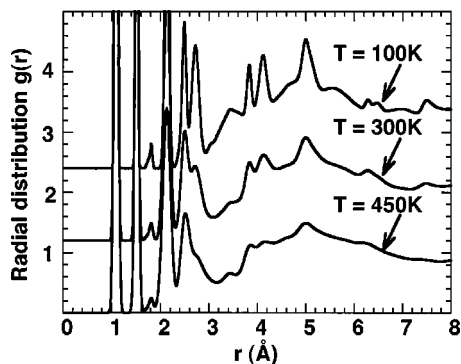


FIG. 7. Calculated radial distribution function,  $g(r)$  at  $T=100$ , 300, and 450 K for  $n=13$ . The curves for  $T=100$  and 300 K are shifted vertically for clarity.

Figure 7 shows the radial distribution function at  $T=100$ , 300, and 450 K. The first three peaks correspond to C-H, C-C, and S-C bond lengths, respectively, whereas the remaining peaks represent the distances beyond the nearest neighbors. With increasing temperature, the positions of the peaks lying within 3 Å remain essentially unchanged but the peaks around 4 and 5 Å almost disappear at 450 K. This implies the absence of long-range order at high temperatures, which is consistent with the loss of rotational order as seen in Fig. 6.

Structural information in  $X$ - $Y$  plane can be probed experimentally using x-ray diffraction<sup>29</sup> and surface x-ray scattering studies.<sup>30</sup> The quantity that is measured experimentally in these studies is the structure factor,

$$S(k) = \frac{1}{N} \langle |\rho(\mathbf{k})|^2 \rangle, \quad (10)$$

where  $\rho(\mathbf{k})$  is the fourier transform of the local particle density,

$$\rho(\mathbf{k}) = \sum_{i=1}^N \exp[-i\mathbf{k}\cdot\mathbf{r}_i] = \sum_{i=1}^N \exp[-i(k_x r_{ix} + k_y r_{iy})] \quad (11)$$

and  $\mathbf{k}=(k_x, k_y, 0)$  represents a two-dimensional scattering vector.

Six peaks of equal intensity are expected in case of just a hexagonal lattice, which is the underlying lattice in case of alkanethiols. However, the internal structure, i.e., planes formed by the  $\text{CH}_2$  units modulates the peaks as shown in Fig. 8(b). In Fig. 8(a) we consider only odd numbered carbons in all chains, so as to get a nearly linear set of atoms along the surface normal (sulfur atoms are not included). We see that in this case, all the six peaks are of equal intensities, as expected. This is in contrast to Fig. 8(b), in which all the atoms in a chain are considered and the planes are parallel to  $x$  axis. The shortening of the peaks at  $K_y=0$ , suggest that the destructive interference due to the plane, reduces the height of peaks. There is an overall increase in the intensity of the all the peaks (height) because of the increased number of atoms included and also the inclusion of sulfur atoms, which contribute heavily to the peaks.

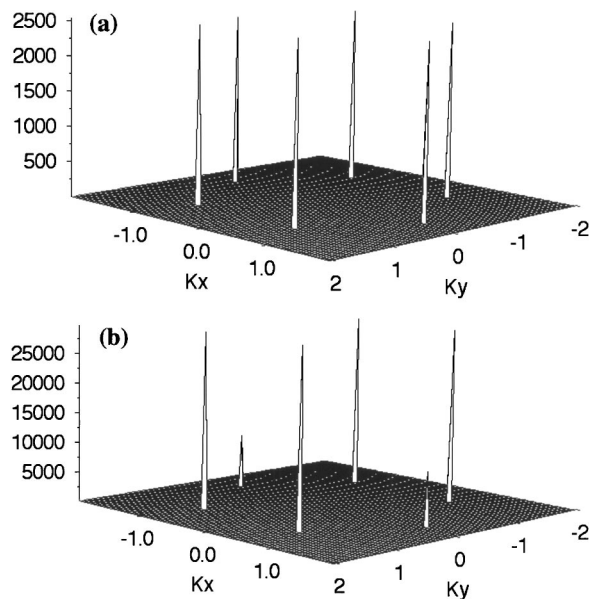


FIG. 8. Calculated structure factors for (a) only odd carbons in a chain are considered (b) all the atoms in the chain, including sulfur, are considered.

In Fig. 9, we show the change in the structure factor with the temperature. Figure 9(a) shows  $S(\mathbf{k})$  with uniform tilt, at temperature of 0 K, whereas Figs. 9(b) and 9(c), show  $S(\mathbf{k})$  at 200 and 400 K, respectively. The peak intensity is a function of both temperature and tilt angle of chains. In case of 200 K, the peak intensity decreases from zero-temperature value because of the disorder due to temperature. But in the case of 400 K, the heights of all the six peaks are almost the same, because of loss of any directionality of the planes (see Fig. 6 for the loss of order in twist angle distribution  $\sim 450$  K). The peak heights also increase because of the untilting of the chains.

The line density profile of backbone atoms normal to the surface gives a measure of the positional order and the calculated profiles at  $T=100, 300, 450$  K are shown in Fig. 10. The presence of a doublet pattern in the density plot at 100 K is an indication of all-trans structure in the backbone plane (the C-C bond takes an alternative sequence of two orientations, nearly parallel and normal, with respect to the surface normal). As temperature increases, the doublet pattern becomes less pronounced, partly due to increased reorientational motion of the backbone planes about the molecular axes and partly due to decreased tilt angle. Above 300 K, the peaks are uniformly spaced and the profiles extend along the  $z$  direction as a result of the untilting. The peaks become broader, indicating a lower degree of positional order of the backbone atoms at high temperatures.

## B. Effect of lattice constant

To study the effect of lattice spacing  $a$  on the tilt structure, we have also performed MD simulations for two additional lattice spacings of 4.7 and 5.3 Å. Figure 11 shows the average tilt angle as a function of lattice spacing for  $T=0, 200$ , and 300 K. The chains do not show any significant tilt when the nearest-neighbor spacing is less than 5 Å. With increased lattice spacing, the collective tilt angle rapidly in-

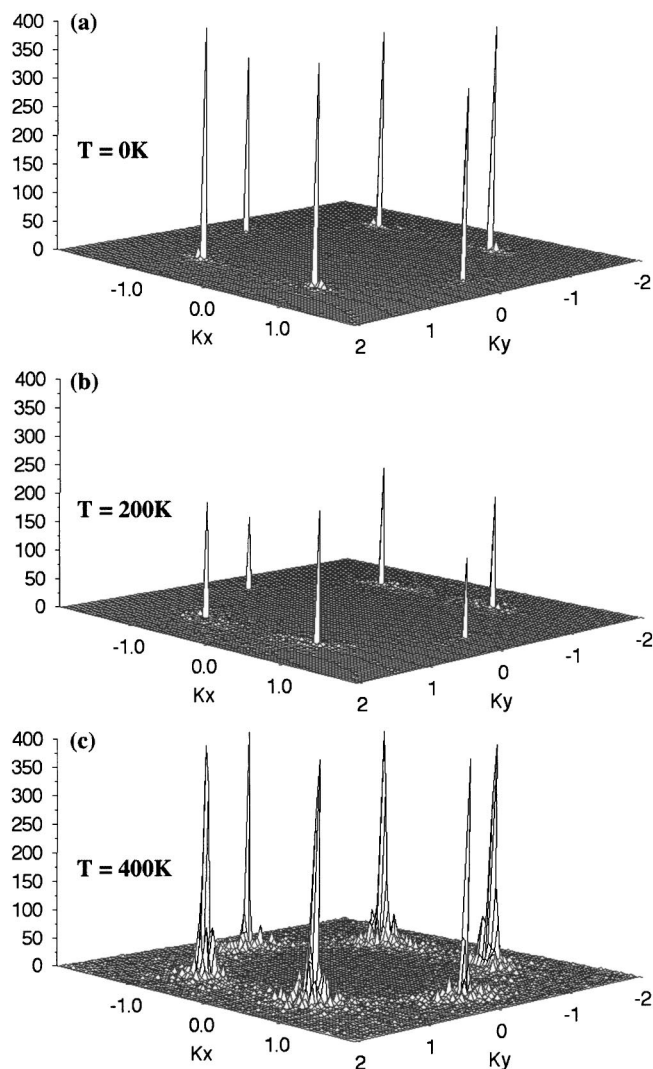


FIG. 9. Calculated structure factors for tilted chains at (a)  $T=0$  K (b)  $T=200$  K (c)  $T=400$  K.

creases, consistent with previous simulations<sup>16</sup> and experiments.<sup>28</sup> Figure 11 shows that the effect of temperature is small for  $a=4.7$  Å but is significant for  $a=5$  Å. Our results also show that the tilt direction and twist angle distribution are insensitive to the lattice spacing.

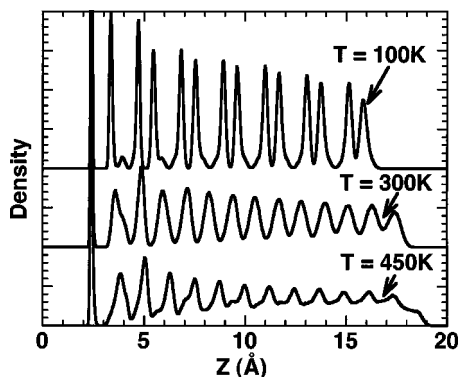


FIG. 10. Calculated density profiles along the surface normal for  $T=100$ , 300, and 450 K for  $n=13$ . The curves for  $T=100$  and 300 K are shifted vertically for clarity.

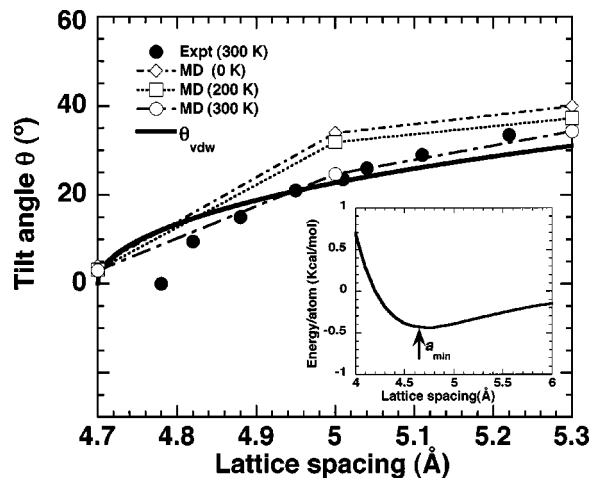


FIG. 11. The collective tilt angle as a function of lattice spacing. The simulation results are shown by diamonds at 0 K, squares at 200 K, and open circles at 300 K. The room temperature experimental data for Langmuir (air/water) monolayer are shown by solid circles. The solid line shows  $\theta_{\text{vdw}}$  [see Eq. (8)]. Shown in the inset is the vdw energy as a function of interchain separation where  $a_{\text{min}}=4.7$  Å.

The effect of lattice spacing on the tilt angle may be understood as follows. As shown in the inset of Fig. 11, the van der Waals interactions as a function of interchain separation has a minimum at  $a_{\text{min}}=4.7$  Å. For SAMs with lattice spacing  $a$ , the van der Waals energy can be minimized by tilting the chains by

$$\theta_{\text{vdw}} = \cos^{-1} \sqrt{\frac{3}{4(a/a_{\text{min}})^2 - 1}}, \quad (12)$$

so that the interchain separation becomes  $a_{\text{min}}$ . The  $\theta_{\text{vdw}}$  plotted in Fig. 11 qualitatively explains the calculated lattice space dependence of the tilt angle.

### C. Effect of molecular chain length

MD simulations are performed for alkanethiol SAMs of different chain lengths  $n$  between 7 and 25. Figure 12 shows the tilt angle as a function of  $n$  for  $T=50$ , 200, and 300 K. At low temperatures, the effect of chain length on tilt angle is negligible. However, at higher temperatures, the tilt angle is an increasing function of  $n$ , and the effect is most pro-

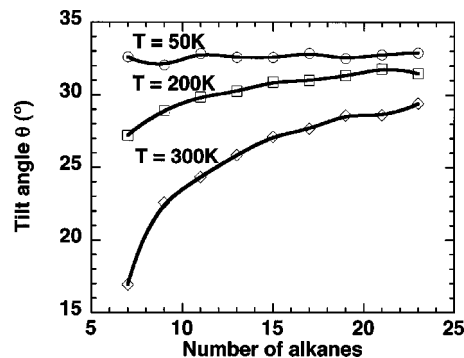


FIG. 12. Tilt angle as a function of chain length for  $T=50$ , 200, and 300 K.

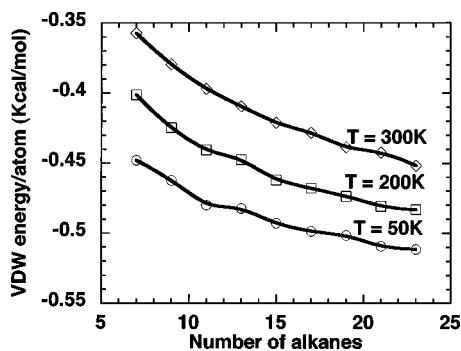


FIG. 13. The van der Waals energy/atom as a function of chain length for  $T=50, 200,$  and  $300$  K.

nounced at  $300$  K. The tilt angle varies with length more for shorter chains ( $n \leq 15$ ) than it does for longer chains ( $n \geq 15$ ).

The above results may be understood as follows. The tilt angle is determined by a competition between potential-energy and entropy contributions to the free energy. The potential energy contribution favors the tilting as discussed previously, see Eq. (12), whereas the entropy contribution favors  $\theta=0$  due to larger available volume for conformational changes. The potential energy contribution consists of van der Waals and surface energy terms. Since the surface potential in the  $z$  axis [second term in Eq. (4)] is short ranged ( $5 \text{ \AA}$  which is much less than the shortest simulated chain length of  $13 \text{ \AA}$  for  $n=7$ ), its contribution to the energy is almost independent of chain length. On the other hand, the magnitude of van der Waals potential energy increases, more negative, as a function of chain length, as shown in Fig. 13. For shorter chains, the surface term dominates the potential energy. However because of the short range nature of the surface term, atoms far from the surface are free to move and hence the entropic contributions are more important at high temperatures. This explains the large variation of tilt angle with temperature for shorter chains as seen in Fig. 12.

We have also observed significant effects of chain length on the existence of gauche defects, i.e., there are more gauche defects in shorter chains than in longer chains. This is seen in Fig. 14, which shows torsion angle distribution of C-C-C-C at  $T=200, 300, 400$  K in the shortest chain length [ $n=7$ , Fig. 14(a)] and in the longest chain length [ $n=23$ , Fig. 14(b)]. Gauche defects ( $g^-$  and  $g^+$ ), which can be seen as peaks at  $\pm 120^\circ$ , start appearing at  $300$  K in  $n=7$  case, while significant gauche peaks are seen only at  $400$  K for  $n=23$ .

We have calculated the chain length dependence of the twist angle distribution. The twist angle distributions for the chain lengths of  $n=7$  and  $23$  for  $T=0, 200$  and  $300$  K are plotted in Fig. 15. At  $300$  K, for  $n=7$  [Fig. 15(a)], the twist angle distribution becomes uniform (chains are free to rotate), whereas some structure remains for  $n=23$  [Fig. 15(b)]. The peak positions are also different for  $n=7$  and  $23$ , even at  $0$  K. We find that for the shorter chain [Fig. 15(a)], the system at  $0$  K is essentially defect free, with only one peak  $\sim -50^\circ$ , but for the case of longer chain [Fig. 15(b)], some twist defects appear even at  $0$  K (small peak  $\sim 125^\circ$ ).

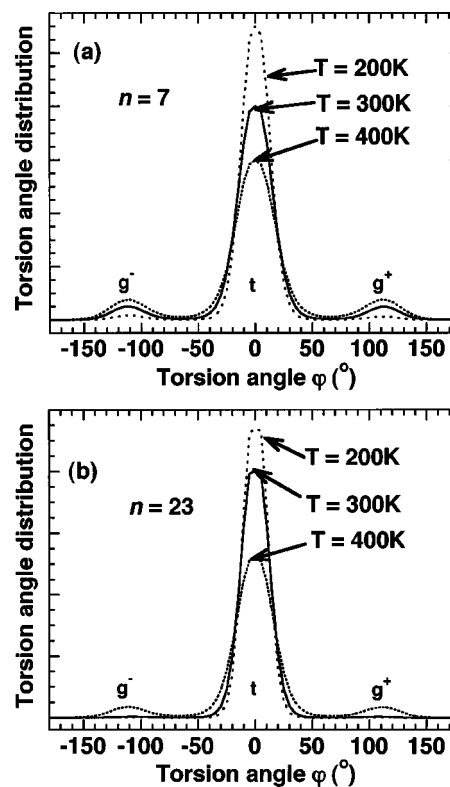


FIG. 14. (a) Torsion angle distribution for  $n=7$  for  $T=200, 300,$  and  $400$  K. (b) Torsion angle distribution for  $n=23$  for  $T=200, 300,$  and  $400$  K. The gauche defects are marked by  $g^-$  and  $g^+$  and trans configuration by  $t$ .

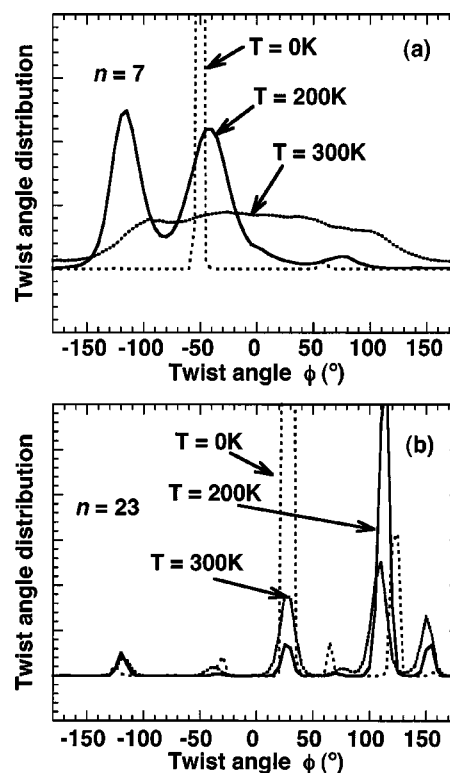


FIG. 15. (a) Twist angle distribution for  $n=7$  for  $T=0, 200,$  and  $300$  K. (b) Twist angle distribution for  $n=23$  for  $T=0, 200,$  and  $300$  K.

#### IV. CONCLUSIONS

Large-scale molecular dynamics simulations of self-assembled alkanethiol monolayer systems have been carried out using an all-atom model to investigate their structural properties as a function of temperature, lattice spacing, and molecular chain length. To perform large-scale simulations reported in this paper, we have developed a scalable parallel MD code, which achieved 90% of the perfect speedup on 1,024 IBM SP4 processors. Our MD simulations for a million atom system of 13-carbon alkane thiolate chains spaced on average 5.0 Å apart on the surface showed that the chains tilt from the surface normal by a collective angle of 25° along next-nearest neighbor direction at 300 K. This is consistent with the experimental result of  $30 \pm 10^\circ$  obtained from IR absorption measurements, but not with the experimental result of  $33.7 \pm 0.8^\circ$  obtained from x-ray diffraction measurements. The tilt structure is found to depend strongly on temperature and exhibits hysteresis. The twist angle distribution is also found to depend on temperature. At 350 K the system transforms to a disordered phase characterized by small collective tilt angle, flexible tilt direction, and random distribution of backbone planes, where the chains are free to rotate. The tilt structure also depends on lattice spacing  $a$ : With increasing lattice spacing, the tilt angle increases rapidly from a nearly zero value at  $a = 4.7 \text{ \AA}$  to as high as  $34^\circ$  at  $a = 5.3 \text{ \AA}$  at 300 K. Finally, the effects of the molecular chain length on the tilt structure are significant at high temperatures.

#### ACKNOWLEDGMENTS

We are thankful to Dr. Grest for many helpful discussions on SAMs. This work was supported by AFOSR-DURINT: USC-Berkeley-Princeton, AFRL, ARL, NASA, NSF, and Louisiana Board of Regents Health Excellence Fund. Simulations were performed at Department of Defense's Major Shared Resource Centers under CHSSI and Challenge projects, and at LSU's Center for Applied Information Technology and Learning (CAPITAL) and Biological Computation and Visualization Center (BCVC).

- <sup>1</sup>F. Schreiber, *Prog. Surf. Sci.* **65**, 151 (2000).
- <sup>2</sup>M. Chandross, G. S. Grest, and M. J. Stevens, *Langmuir* **18**, 8392 (2002).
- <sup>3</sup>K. L. Prime and G. M. Whitesides, *Science* **252**, 1164 (1991).
- <sup>4</sup>R. G. Nuzzo, L. H. Dubois, and D. L. Allara, *J. Am. Chem. Soc.* **112**, 558 (1990).
- <sup>5</sup>M. D. Porter, T. B. Bright, D. L. Allara, and C. E. D. Chidsey, *J. Am. Chem. Soc.* **109**, 3559 (1987).
- <sup>6</sup>C. E. D. Chidsey and D. N. Loiacono, *Langmuir* **6**, 682 (1990).
- <sup>7</sup>L. Strong and G. M. Whitesides, *Langmuir* **4**, 546 (1988).
- <sup>8</sup>R. G. Nuzzo, E. M. Korenic, and L. H. Dubois, *J. Chem. Phys.* **93**, 767 (1990).
- <sup>9</sup>P. Fenter, P. Eisenberger, and K. S. Liang, *Phys. Rev. Lett.* **70**, 2447 (1993).
- <sup>10</sup>N. Camillone III, C. E. D. Chidsey, G. Y. Liu, and G. Scoles, *J. Chem. Phys.* **98**, 3503 (1993).
- <sup>11</sup>G. E. Poirier and M. J. Tarlov, *Langmuir* **10**, 2853 (1994).
- <sup>12</sup>P. Fenter, P. Eisenberger, and K. S. Liang, *J. Chem. Phys.* **106**, 1600 (1997).
- <sup>13</sup>A. Ulman, *J. Mater. Educ.* **11**, 205 (1989).
- <sup>14</sup>J. Hautman and M. L. Klein, *J. Chem. Phys.* **91**, 4994 (1989); **93**, 7483 (1990).
- <sup>15</sup>J. P. Bareman and M. L. Klein, *J. Phys. Chem.* **94**, 5200 (1990).
- <sup>16</sup>W. Mar and M. L. Klein, *Langmuir* **10**, 188 (1994).
- <sup>17</sup>A. J. Pertsin and M. Grunze, *Langmuir* **10**, 3668 (1994).
- <sup>18</sup>R. Bhatia and B. J. Garrison, *Langmuir* **13**, 765 (1997); **13**, 4038 (1997).
- <sup>19</sup>R. A. Sorensen, W. B. Liao, L. Kesner, and R. H. Boyd, *Macromolecules* **21**, 200 (1988).
- <sup>20</sup>W. L. Jorgensen, *J. Phys. Chem.* **90**, 6379 (1986).
- <sup>21</sup>M. P. Allen and D. J. Tildesley, *Computer Simulation of Liquids* (Oxford University Press, Oxford, 1987).
- <sup>22</sup>A. Nakano, R. K. Kalia, and P. Vashishta, *Comput. Phys. Commun.* **83**, 197 (1994).
- <sup>23</sup>G. J. Martyna, M. E. Tuckerman, D. J. Tobias, and M. L. Klein, *Mol. Phys.* **87**, 1117 (1996).
- <sup>24</sup>M. Tuckerman, B. J. Berne, and G. J. Martyna, *J. Chem. Phys.* **97**, 1990 (1992).
- <sup>25</sup>S. Vemparala, R. K. Kalia, B. B. Karki, A. Nakano, and P. Vashishta, *Parallel Computing* (submitted).
- <sup>26</sup>R. G. Nuzzo, E. M. Korenic, and L. H. Dubois, *J. Chem. Phys.* **93**, 767 (1990).
- <sup>27</sup>L. H. Dubois, B. R. Zegarski, and R. G. Nuzzo, *J. Chem. Phys.* **98**, 678 (1993).
- <sup>28</sup>K. Kjaer, J. Als-Nielsen, C. A. Helm, P. Tippman-Krayer, and H. Mohwald, *J. Phys. Chem.* **93**, 3200 (1989).
- <sup>29</sup>K. Kjaer, J. Als-Nielsen, C. A. Helm, L. A. Laxhuber, and H. Mohwald, *Phys. Rev. Lett.* **58**, 2224 (1987).
- <sup>30</sup>P. Dutta, J. B. Peng, B. Lin, J. B. Ketterson, M. Prakash, P. Georgopoulos, and S. Ehrlich, *Phys. Rev. Lett.* **58**, 2228 (1987).